GEOLOGY | THE GEOLOGICAL SOCIETY OF AMERICA®

https://doi.org/10.1130/G45429.1

Manuscript received 27 July 2018
Revised manuscript received 22 October 2018
Manuscript accepted 25 October 2018

Published online 9 November 2018

A trapdoor mechanism for slab tearing and melt generation in the northern Andes

Gideon Rosenbaum[1], Mike Sandiford[2], John Caulfield[1], and Jennifer M. Garrison[3]
[1]School of Earth and Environmental Sciences, The University of Queensland, Brisbane, QLD 4072, Australia
[2]School of Earth Sciences, University of Melbourne, Carlton, VIC 3053, Australia
[3]Department of Geological Sciences, California State University, Los Angeles, California 90032, USA

ABSTRACT

Segments of flat subduction are recognized in subduction zones, but little is known about the behavior of slabs along the edges of flat slab segments. Well-constrained earthquake data from the northern edge of the Peru flat slab segment reveal that the subducting Nazca slab is more contorted than previously assumed, with a prominent tear developed along a lateral ramp that bounds the Peruvian flat slab beneath southern Ecuador. The slab geometry and associated tear are spatially linked to Sumaco volcano ~100 km east of the arc front. Sumaco mafic lavas are ultrapotassic, enriched in incompatible elements, and show little evidence for crustal assimilation. These geochemical signatures are consistent with low-degree (≤3%) melting of an upper mantle source comprising depleted mid-oceanic ridge basalt (MORB) mantle within the spinel stability field, and metasomatism of the source by melts derived from the basaltic portion of the slab within the garnet stability field (>80 km depth). We propose that focused melting at the slab edge was enabled by the combination of tearing and the generation of poloidal mantle flow in the proximity of the tear. A possible explanation for this process is the opening of a trapdoor-style tear, which induced a poloidal mantle flow by the gravitational foundering of the relatively old and dense edge of the flat slab segment.

INTRODUCTION

Subducting oceanic lithosphere deforms in complex ways by bending, stretching, and tearing. While such complexities are known to be fundamental to the character and distribution of volcanic activity along convergent margins (e.g., Gvirtzman and Nur, 1999; Yogodzinski et al., 2001), their three-dimensional geometry is relatively poorly constrained. For example, global slab models (e.g., Hayes et al., 2012), which extrapolate earthquake data to construct a continuous slab, inevitably oversimplify discontinuities in the slab geometry, such as slab tearing and segmentation.

The origins of flat slabs have been postulated to be caused by changes in the mechanical coupling between the subducting and overriding plates in response to the subduction of buoyant material, mantle wedge suction, thickened overriding plate, or forced trench retreat (e.g., van Hunen et al., 2000; Manea et al., 2012). One such example is the Peru flat slab (Fig. 1), which occurs in the area where a prominent anomaly in the oceanic Nazca plate (Nazca Ridge) has been subducted (Gutscher et al., 2000; Hu and Liu, 2016). The flat slab segment coincides with a gap in arc volcanism and is characterized by a shallowly dipping slab that becomes sub-horizontal at ~100 km depth (Gutscher et al., 2000). Anomalously thick oceanic crust also occurs offshore of Chile and Ecuador, leading to the subduction of the Juan Fernandez Ridge and Carnegie Ridge, respectively (Fig. 1), but subduction of the latter does not coincide with a gap in arc volcanism. Rather, a chain of volcanoes 250–300 km east of the trench (Fig. 2A) indicates that the slab segment beneath Ecuador reaches sufficient depths (>120 km) that allow melt production in the overlying mantle wedge. Relatively low seismicity rates in northern Ecuador mean that the geometry of the subducted slab is poorly constrained. Therefore, the question of how deformation is accommodated as the slab changes its configuration, from flat-slab subduction in northern Peru to a more steeply-dipping regime beneath Ecuador, has remained controversial (Gutscher et al., 1999; Michaud et al., 2009; Yepes et al., 2016). In this study, using a combination of seismological and geochemical data, we address this issue by providing better constraints on the geometry of the subducting slab beneath the northern Andes and the magmatic response to slab deformation.

STRUCTURE OF THE ECUADORIAN SLAB

To constrain the slab geometry in the northern Andes, we use earthquake data from the ISC-EHB Bulletin (http://www.isc.ac.uk/isc-ehb/) and the Global Centroid-Moment-Tensor (CMT) catalogue (https://www.globalcmt.org) (see the GSA Data Repository[1] for details). These data allow us to test the assumption integrated in the slab models (Hayes et al., 2012; Hayes, 2018) that entails a gently curved and continuous lateral ramp in the area where slab contours are bent (Figs. 1 and 2A), and to infer processes that potentially cause fragmentation between the flat northern Peru and steeper Ecuador segments.

Despite low levels of slab seismicity in southern Colombia and northern Ecuador, the ISC-EHB data constrain the slab geometry in a cross section (Fig. 2B), showing an east-dipping slab subducting at ~30° beneath the Northern Andean Volcanic Zone. In contrast, a section through the volcanic gap (latitude 3–5°S) shows that the slab flattens at ~100 km depth (Fig. 2C). The change in the slab dip angle, at approximately latitude 1–2°S, is demonstrated in a section parallel to the plate boundary (Fig. 2D), which shows that the northern and southern flat slab segments are separated by a seismic gap. The section also shows a cluster of deeper (180–220 km) earthquakes (El Puyo Seismic Cluster; Yepes et al., 2016), which occurs below the lower bound of the slab model (Fig. 2D).

[1]GSA Data Repository item 2018418, detailed methods, Figures DR1 and DR2, and Tables DR1and DR2, is available online at http://www.geosociety.org/datarepository/2018/, or on request from editing@geosociety.org.

CITATION: Rosenbaum, G., Sandiford, M., Caulfield, J., and Garrison, J.M., 2018, A trapdoor mechanism for slab tearing and melt generation in the northern Andes: Geology, v. 47, p. 23–26, https://doi.org/10.1130/G45429.1

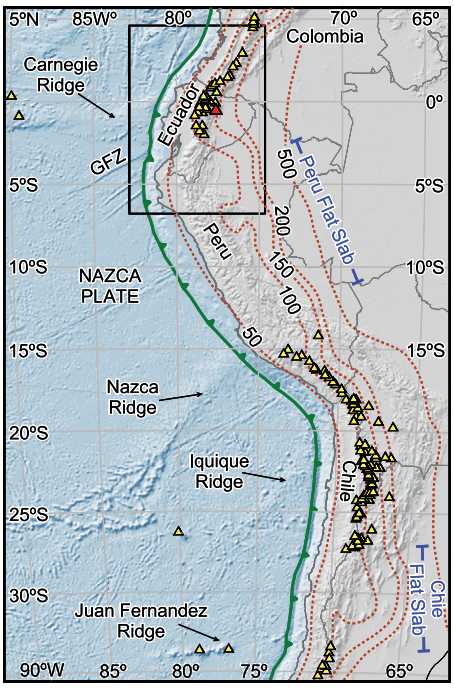

Figure 1. Map showing bathymetric highs in the subducting Nazca Plate, active volcanoes (yellow triangles; red triangle is Sumcao volcano), and flat slab segments. Dashed brown lines are slab depth contours (in kilometers; after Hayes, 2018). GFZ—Grijalva Fracture Zone.

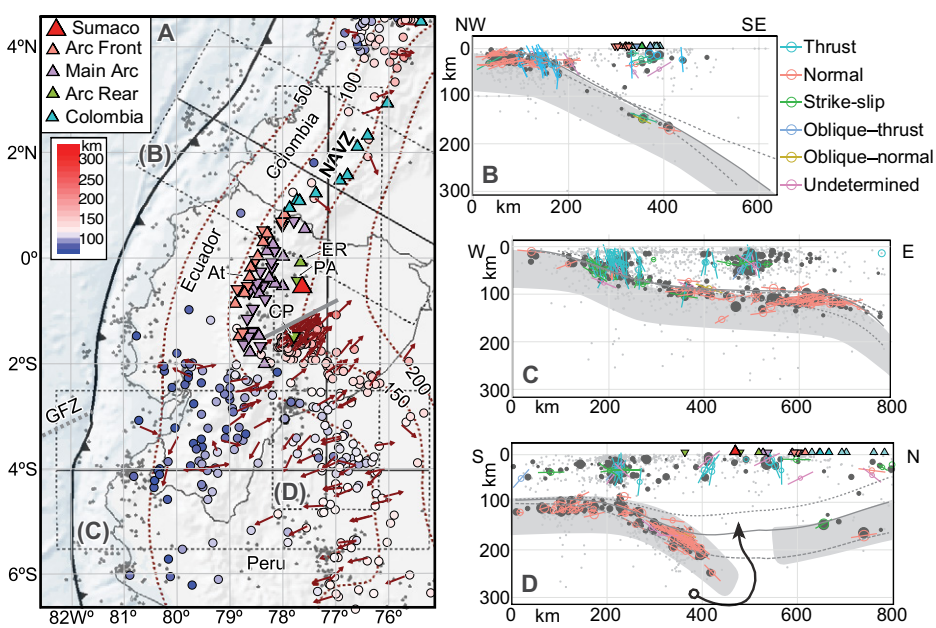

Figure 2. A: Seismicity from the ISC-EHB bulletin (http://www.isc.ac.uk/isc-ehb/). Colored circles indicate earthquakes at 70–340 km depth; events outside this range are shown by gray dots. Triangles and inverted triangles indicate active (Holocene) and extinct (Pleistocene) volcanoes, respectively (see Table DR1 [see footnote 1] for the full list of volcanoes). Thick gray line indicates an abrupt change in seismic behavior along a boundary striking 070. Brown arrows indicate Centroid-Moment-Tensor (CMT) T-axes (tension; for events >70 km). Abbreviations: At—Atacazo volcano; CP—Conos de Puyo volcano; ER—El Reventador volcano; GFZ—Grijalva Fracture Zone; NAVZ—North Andean Volcanic Zone; PA—Pan de Azucar volcano. B–D: Cross sections showing projected CMT T-axes (colored open circles and lines) and hypocenters from the ISC-EHB bulletin (black circles, scaled to magnitudes in the range of M_w 3.5–8) and ISC catalogue (gray dots). Solid and dashed lines show the Slab2 Model (Hayes, 2018) along the central axis and edges, respectively, of the profile boxes. The shading represents an interpretation of the slab geometry along the central axis of the swath (assuming slab thickness of 75 km).

The occurrence of progressively deeper earthquakes from latitude 3°S to El Puyo Seismic Cluster (Fig. 2A; Fig. DR1A in the Data Repository) indicates that in this area, the slab dip angle has a northward component (Fig. 2D). Furthermore, by analyzing the deviation of ISC-EHB hypocenters from the expected depths of the slab model (Figs. DR1B and DR1C), one can recognize a prominent asymmetry, associated with an abrupt change from earthquakes steeper than the slab model (at latitude 1–2°S) to earthquakes that are anomalously shallow (at latitude 2–3°S). These deviations indicate that the slab in this area is more strongly curved than implied by the slab model.

Analysis of T-axes (tension) derived from the CMT catalogue (Fig. 2; Fig. DR2) provides an additional insight into the active deformation within the slab. Along the Peru flat slab segment, the recognition of ENE-WSW sub-horizontal T-axes implies stretching along the upper part of the slab in the subduction direction. In southern Ecuador, T-axes rotate and steepen into a northeast-plunging trend, oblique to subduction (Figs. 2A and 2D). This observation supports the suggestion that the northern edge of the Peru flat slab segment is contorted (Yepes et al., 2016), with the edge of the flat slab forming a lateral ramp adjacent to a portion of the slab that is dipping to the northeast. This zone of slab deformation occurs immediately south of Sumaco volcano.

ORIGIN OF SUMACO VOLCANO

The unique geochemical characteristics of Sumaco volcano and its peculiar location >100 km east of the arc front provide information on the processes operating at the edge of the flat slab segment. Sumaco lavas have unusual geochemical characteristics (Barragan et al., 1998; Bryant et al., 2006; Garrison et al., 2018) including low silica content (43–55 wt%), high alkalinity ($K_2O + Na_2O$ = 2.4–12.6 wt%; Fig. 3A), and strong enrichment in incompatible elements (Fig. 3B). While the majority of Ecuadorian lavas typically have intermediate calc-alkaline affinities, the high alkalinity basanite to tephriphonolite character of Sumaco distinguishes it from all other active Ecuadorian volcanoes (including the backarc volcanoes of Conos de Puyo, Pan de Azucar, and El Reventador; Fig. 2A; cf. Table DR2 for the Ecuadorian data compilation).

The occurrence of basic and ultrabasic lavas in the backarc, most notably at Sumaco, suggests a relatively primitive mantle-derived parental melt largely unaffected by crustal assimilation. $^{207}Pb/^{204}Pb$ values in Sumaco (15.575–15.618) overlap values for arc-front lavas, whereas $^{206}Pb/^{204}Pb$ values (18.792–18.928) are less radiogenic than arc-front lavas. Along with arc-front lavas, Sumaco is the least radiogenic Sr ($^{87}Sr/^{86}Sr$ = 0.704043–0.704399) and most radiogenic Nd ($^{143}Nd/^{144}Nd$ = 0.512868–0.512926) of the Ecuadorian arc array (Barragan et al., 1998; Bourdon et al., 2003; Bryant et al., 2006; Chiaradia et al., 2009; Ancellin et al., 2017; Garrison et al., 2018). The Nd isotopic compositions overlap those of the Galapagos Islands and Carnegie Ridge basalts. Taken together, the isotopic constraints imply an upper mantle source similar to that inferred for the arc front (Ancellin et al., 2017), but with lower degrees of crustal assimilation (Bryant et al., 2006). The presence of sector-zoned titanaugite crystals, high inferred magmatic temperatures (1000–1100 °C), and the elevated sulfur contents (up to 843 ppm) of Sumaco lavas (Garrison et al., 2018) imply rapid melt transport from the source with insufficient time for degassing.

Very low-degree partial melting of a metasomatized asthenospheric mantle can account for enrichments in the incompatible elements K, Rb, Th, and U in Sumaco (e.g., Barragan et al., 1998), while elevated Nb and Ta relative to the Ecuadorian arc front imply a contribution from a high field strength element (HFSE)–rich

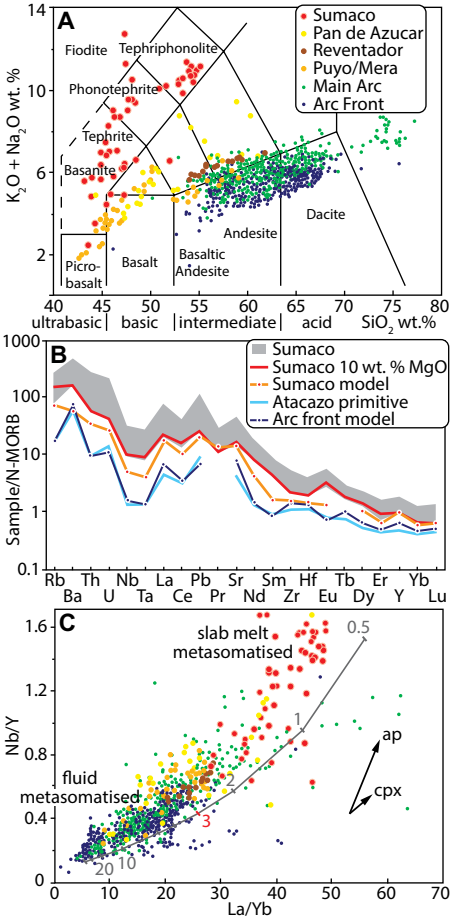

Figure 3. Geochemistry of Sumaco volcano (Ecuador) in comparison to rocks from other Ecuadorian volcanoes (for data and references, see Table DR2 [see footnote 1]). A: Total alkali versus silica classification diagram. B: Normal mid-oceanic ridge basalt (N-MORB) normalized incompatible multi-element diagram showing range of Sumaco compositions, 10 wt% MgO Sumaco basanite, and the modeled Sumaco primary melt. Included for comparison are a primitive arc-front composition from Atacazo volcano and the modeled arc-front melt. C: Plot of Nb/Y versus La/Yb (after Hoffer et al., 2008) including the melting trajectory for the estimated Sumaco source (gray line, depleted MORB mantle [DMM] + 2% slab melt). Tick marks denote extent of melting (%), with 3% melting (red) inferred for the primary Sumaco melt. Arrows represent mineral Rayleigh fractionation vectors for 30% apatite (ap) and 40% clinopyroxene (cpx) crystallization.

reservoir (Fig. 3B). In the case of potassic arc rocks, this has been inferred to reflect addition of a slab-derived melt (Stolz et al., 1996). Additionally, extremely high Sr abundances require an enriched component relative to the upper mantle and subduction fluids (e.g., Bourdon et al., 2003). The isotope systematics preclude an enriched mantle source (Bryant et al., 2006; Hidalgo et al., 2012; Ancellin et al., 2017), and a negligible role for assimilation rules out lower crustal melting. In terms of slab contributions, the low Ba/La (14–21) and Ba/Th (72–171) relative to arc front and other backarc lavas imply little dehydration fluid contribution (Ba/La = 20–80, Ba/Th = 81–526). Similarly, low Th/Ce (0.06–0.15) compared to the rest of the arc system (0.03–0.5) is consistent with negligible sediment input (Hawkesworth et al., 1997). We consider the enriched signatures at Sumaco to reflect an asthenospheric mantle source metasomatized by partial melts of subducting Carnegie Ridge basalts, as previously suggested for adakite-like magmas in Ecuador (Bourdon et al., 2002; Hoffer et al., 2008; Hidalgo et al., 2012). Comparison of model results with the incompatible trace element profile of the most primitive Sumaco basanite (Fig. 3B) indicates that the proportion of slab melt added to the source is small (~2%), and the degree of melting very low (≤3%), in accordance with the inferred negligible fluid contribution and the marked enrichment in the most incompatible elements (for the full geochemical model, see the Data Repository). As noted previously for Conos de Puyo (Hoffer et al., 2008), slab melts are enriched relative to fluids, making them effective metasomatic agents, while highly alkaline, low-viscosity mafic melts allow segregation from the source region, despite low degrees of partial melting. Crucially, the model (Fig. 3B) reproduces the elevated Rb, Th, U, Nb, Ta, light rare earth element (LREE), Pb, and Sr contents of the Sumaco rocks relative to the arc front.

Ecuadorian arc front lavas are inferred to contain components of slab-derived fluids, sediment melts, and melts of the basaltic oceanic crust, the proportions of which vary with latitude (Ancellin et al., 2017). In order to compare the mantle source beneath the arc front with that for Sumaco, we selected Atacazo volcano (Fig. 2A), which shares similar Sr-Nd-Pb isotopic signatures (Ancellin et al., 2017). The modeled Atacazo source comprises a bulk mixture of 93% depleted mid-oceanic ridge basalt (MORB) mantle (DMM), 1% slab melt, 3% slab derived fluid, and 3% sediment melt. A 10% melt of this source, in accordance with Ecuadorian arc-front estimates (Ancellin et al., 2017) in the spinel stability field, closely reproduces the incompatible trace element profile of the primitive Atacazo endmember (Fig. 3B). Arc-front lavas show overall lower trace element concentrations, particularly for the most incompatible elements (e.g., Rb, Th, U); depletions in Ba and Sr are less pronounced, likely reflecting the increased role of fluids proximal to the trench. The Sumaco melting model is depicted on a plot of Nb/Y versus La/Yb, together with compiled Ecuadorian arc and backarc data (Fig. 3C). Unlike subduction fluids, slab melts are able to mobilize HFSEs, such as Nb (Hoffer et al., 2008), and at the same time impart elevated LREE/HREE (heavy REE) signatures due to residual garnet (Bourdon et al., 2003). The model melting trajectory demonstrates that the Sumaco rocks require much lower degrees of partial melting (≤3%) to generate the inferred primary melt (Nb/Y = 0.42, La/Yb = 26). Together with Ba/Th and Ba/La systematics, these observations highlight the decreasing role of fluids across the arc. While the more-evolved arc front and main arc lavas reflect assimilation and fractional crystallization processes, these suites show the strongest fluid signatures, with backarc samples spanning a broad range of compositions recording variable metasomatic contributions. Notably, lavas from Pan de Azucar that plot within the high-Nb/Y, high-La/Yb Sumaco field, suggest that this now-extinct backarc volcano close to Sumaco (Fig. 2A) experienced a similar melt-generation regime in the past. Significantly, with negligible influence of slab fluids, slab melts alone are shown to be responsible for generating mantle melting beneath Sumaco, a process that is currently restricted to this volcanic center.

The phonolitic composition of Sumaco rocks is unique within the Ecuadorian arc system. Alkaline magmas are typically associated with low-degree decompression melting in plume or rift-related settings (Takahashi and Kushiro, 1983). In our model, the preservation of highly alkaline primary melts is explained by low-degree melting in the spinel stability field (<80 km) and a rapid ascent through thickened overriding crust (up to 60 km). Decompression melting, triggered by rapid ascent from the source region, may have also played a role.

DISCUSSION AND CONCLUSIONS

The observations of well-constrained hypocenters below and above the bounds of the slab model (at latitudes 1°S and 2°S, respectively) imply a contorted slab geometry (Yepes et al., 2016), characterized by an asymmetric antiformal lateral ramp and a narrow northeast-dipping limb (Fig. 4A). The termination of seismic activity along a line trending 070 (Fig. 2A) marks an abrupt transition to a zone of no seismicity (Fig. 2D). This seismic boundary coincides with the projected continuation of the Grijalva Fracture Zone (GFZ), marking a transition between an older oceanic lithosphere in the south and a younger lithosphere north of the fracture zone (Yepes et al., 2016; Ancellin et al. 2017). A plausible explanation for the abrupt change in the seismic behavior is the existence of a tear in the slab, which may have developed, along the subducted portion of the GFZ, in response to the deformation associated with the evolution of the Peru flat slab segment (e.g., Hu and Liu, 2016).

The position of Sumaco volcano, immediately above the seismic gap and north of the distorted slab segment (Figs. 2D and 4A), together with the seismic and geochemical observations, may suggest that melt generation was linked

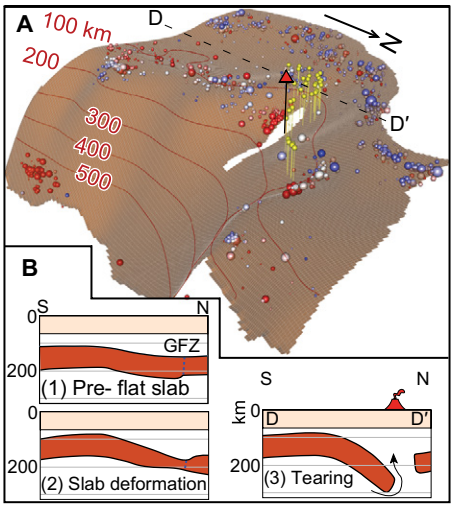

Figure 4. A: Three-dimensional model showing the location of Sumaco volcano, Ecuador (red triangle) above a slab tear (other volcanoes are indicated by yellow markers). Balls indicate relative locations of hypocenters above (blue) or below (red) the Slab2 Model (Hayes, 2018). D-D′ is the cross section location shown in B(3) (cf. Fig. 2D). B: Schematic cross sections showing (1) an early (pre- flat slab) stage with a lithospheric thickness contrast across the subducted Grijalva Fracture Zone (GFZ, dashed line); (2) slab deformation associated with stretching and antiformal bowing; and (3) trapdoor-style tearing that induces poloidal mantle flow underneath Sumaco volcano.

to the mantle dynamics in the proximity of the sinking slab edge. While slab tearing does not necessarily cause magmatism (e.g., Rosenbaum and Piana Agostinetti, 2015), anomalous melting may occur if tearing is accompanied by mantle flow around the slab edge (Gvirtzman and Nur, 1999; Yogodzinski et al., 2001). We propose that the progressive sinking of the older and denser lithosphere south of the GFZ induced a poloidal flow in the proximity of the northeast-dipping slab edge, thus allowing mantle advection through the tear. A trapdoor mechanism may provide a possible analog for this process (Fig. 4B), involving initial stretching and bending of the slab (in response to the progressive flattening of the Peru slab segment), followed by tearing that allowed its foundering. The opening of such a trapdoor must have been compensated by a poloidal mantle flow that facilitated melting of young (12–20 Ma), warm Carnegie Ridge basaltic crust.

We conclude that the localization of geochemically anomalous lavas at Sumaco volcano is intrinsically linked to the spatial extent of the identified tear structure. Slab tearing, in conjunction with focused poloidal mantle flow, increased the propensity for slab melting and the rapid ascent of low-viscosity alkaline melt.

ACKNOWLEDGMENTS

The manuscript benefited from comments by three anonymous reviewers and an informal review by W. Schellart and S. Turner.

REFERENCES CITED

Ancellin, M.-A., Samaniego, P., Vlastélic, I., Nauret, F., Gannoun, A., and Hidalgo, S., 2017, Across-arc versus along-arc Sr-Nd-Pb isotope variations in the Ecuadorian volcanic arc: Geochemistry Geophysics Geosystems, v. 18, p. 1163–1188, https://doi.org/10.1002/2016GC006679.

Barragan, R., Geist, D., Hall, M., Larson, P., and Mark, K., 1998, Subduction controls on the compositions of lavas from the Ecuadorian Andes: Earth and Planetary Science Letters, v. 154, p. 153–166, https://doi.org/10.1016/S0012-821X(97)00141-6.

Bourdon, E., Eissen, J.-P., Monzier, M., Robin, C., Martin, H., Cotten, J., and Hall, M.L., 2002, Adakite-like lavas from Antisana Volcano (Ecuador): Evidence for slab melt metasomatism beneath the Andean Northern Volcanic Zone: Journal of Petrology, v. 43, p. 199–217, https://doi.org/10.1093/petrology/43.2.199.

Bourdon, E., Eissen, J.-P., Gutscher, M.-A., Monzier, M., Hall, M.L., and Cotten, J., 2003, Magmatic response to early aseismic ridge subduction: The Ecuadorian margin case (South America): Earth and Planetary Science Letters, v. 205, p. 123–138, https://doi.org/10.1016/S0012-821X(02)01024-5.

Bryant, J.A., Yogodzinski, G.M., Hall, M.L., Lewicki, J.L., and Bailey, D.G., 2006, Geochemical constraints on the origin of volcanic rocks from the Andean Northern Volcanic Zone, Ecuador: Journal of Petrology, v. 47, p. 1147–1175, https://doi.org/10.1093/petrology/egl006.

Chiaradia, M., Müntener, O., Beate, B., and Fontignie, D., 2009, Adakite-like volcanism of Ecuador: Lower crust magmatic evolution and recycling: Contributions to Mineralogy and Petrology, v. 158, p. 563–588, https://doi.org/10.1007/s00410-009-0397-2.

Garrison, J.M., Sims, K.W.W., Yogodzinski, G.M., Escobar, R.D., Scott, S., Mothes, P., Hall, M.L., and Ramon, P., 2018, Shallow-level differentiation of phonolitic lavas from Sumaco Volcano, Ecuador: Contributions to Mineralogy and Petrology, v. 173, https://doi.org/10.1007/s00410-017-1431-4.

Gutscher, M.A., Malavieille, J., Lallemand, S., and Collot, J.Y., 1999, Tectonic segmentation of the North Andean margin: Impact of the Carnegie Ridge collision: Earth and Planetary Science Letters, v. 168, p. 255–270, https://doi.org/10.1016/S0012-821X(99)00060-6.

Gutscher, M.A., Spakman, W., Bijwaard, H., and Engdahl, E.R., 2000, Geodynamics of flat subduction: Seismicity and tomographic constraints from the Andean margin: Tectonics, v. 19, p. 814–833, https://doi.org/10.1029/1999TC001152.

Gvirtzman, Z., and Nur, A., 1999, The formation of Mount Etna as the consequence of slab rollback: Nature, v. 401, p. 782–785, https://doi.org/10.1038/44555.

Hawkesworth, C.J., Turner, S.P., McDermott, F., Peate, D.W., and van Calsteren, P., 1997, U-Th isotopes in arc magmas: implications for element transfer from the subducted crust: Science, v. 276, p. 551–555, https://doi.org/10.1126/science.276.5312.551.

Hayes, G., 2018, Slab2—A Comprehensive Subduction Zone Geometry Model: U.S. Geological Survey data release, https://doi.org/10.5066/F7PV6JNV.

Hayes, G.P., Wald, D.J., and Johnson, R.L., 2012, Slab1.0: A three-dimensional model of global subduction zone geometries: Journal of Geophysical Research: Solid Earth, v. 117, B01302, https://doi.org/10.1029/2011JB008524.

Hidalgo, S., Gerbe, M.C., Martin, H., Samaniego, P., and Bourdon, E., 2012, Role of crustal and slab components in the Northern Volcanic Zone of the Andes (Ecuador) constrained by Sr-Nd-O isotopes: Lithos, v. 132–133, p. 180–192, https://doi.org/10.1016/j.lithos.2011.11.019.

Hoffer, G., Eissen, J.-P., Beate, B., Bourdon, E., Fornari, M., and Cotten, J., 2008, Geochemical and petrological constraints on rear-arc magma genesis processes in Ecuador: The Puyo cones and Mera lavas volcanic formations: Journal of Volcanology and Geothermal Research, v. 176, p. 107–118, https://doi.org/10.1016/j.jvolgeores.2008.05.023.

Hu, J., and Liu, L., 2016, Abnormal seismological and magmatic processes controlled by the tearing South American flat slabs: Earth and Planetary Science Letters, v. 450, p. 40–51, https://doi.org/10.1016/j.epsl.2016.06.019.

Manea, V.C., Pérez-Gussinyé, M., and Manea, M., 2012, Chilean flat slab subduction controlled by overriding plate thickness and trench rollback: Geology, v. 40, p. 35–38, https://doi.org/10.1130/G32543.1.

Michaud, F., Witt, C., and Royer, J.Y., 2009, Influence of the subduction of the Carnegie volcanic ridge on Ecuadorian geology: Reality and fiction, *in* Kay, S.M., et al., eds., Backbone of the Americas: Shallow Subduction, Plateau Uplift, and Ridge and Terrane Collision: Geological Society of America Memoirs, v. 204, p. 217–228, https://doi.org/10.1130/2009.1204(10).

Rosenbaum, G., and Piana Agostinetti, N., 2015, Crustal and upper mantle responses to lithospheric segmentation in the northern Apennines: Tectonics, v. 34, https://doi.org/10.1002/2013TC003498.

Stolz, A., Jochum, K., Spettel, B., and Hofmann, A., 1996, Fluid-and melt-related enrichment in the subarc mantle: Evidence from Nb/Ta variations in island-arc basalts: Geology, v. 24, p. 587–590, https://doi.org/10.1130/0091-7613(1996)024<0587:FAMREI>2.3.CO;2.

Takahashi, E., and Kushiro, I., 1983, Melting of a dry peridotite at high pressures and basalt magma genesis: The American Mineralogist, v. 68, p. 859–879.

van Hunen, J., van der Berg, A.P., and Vlaar, N.J., 2000, A thermo-mechanical model of horizontal subduction below an overriding plate: Earth and Planetary Science Letters, v. 182, p. 157–169, https://doi.org/10.1016/S0012-821X(00)00240-5.

Yepes, H., Audin, L., Alvarado, A., Beauval, C., Aguilar, J., Font, Y., and Cotton, F., 2016, A new view for the geodynamics of Ecuador: Implication in seismogenic source definition and seismic hazard assessment: Tectonics, v. 35, p. 1249–1279, https://doi.org/10.1002/2015TC003941.

Yogodzinski, G.M., Lees, J.M., Churikova, T.G., Dorendorf, F., Wöerner, G., and Volynets, O.N., 2001, Geochemical evidence for the melting of subducting oceanic lithosphere at plate edges: Nature, v. 409, p. 500–504, https://doi.org/10.1038/35054039.

Printed in USA